



Published in final edited form as:

Nat Cell Biol. 2014 September ; 16(9): 909–917. doi:10.1038/ncb3026.

An extracellular matrix-specific GEF-GAP interaction regulates Rho GTPase crosstalk for 3D collagen migration

Matthew L. Kutys¹ and Kenneth M. Yamada¹

¹Laboratory of Cell and Developmental Biology, National Institute of Dental and Craniofacial Research, National Institutes of Health

Rho-family GTPases govern distinct types of cell migration on different extracellular matrix (ECM) proteins in tissue culture or 3D matrix¹⁻³. We searched for mechanisms selectively regulating 3D cell migration in different matrix environments^{4, 5} and discovered a form of Cdc42-RhoA crosstalk governing cell migration through a specific pair of GTPase activator and inhibitor molecules. We first identified β Pix, a guanine nucleotide exchange factor (GEF), as a specific regulator of migration in 3D collagen using an affinity precipitation-based GEF screen. Knockdown of β Pix specifically blocks cell migration in fibrillar collagen microenvironments, leading to hyperactive cellular protrusion accompanied by increased collagen matrix contraction. Live FRET imaging and RNAi knockdown linked this β Pix knockdown phenotype to loss of polarized Cdc42 but not Rac1 activity, accompanied by enhanced, de-localized RhoA activity. Mechanistically, collagen phosphoregulates β Pix leading to its association with srGAP1, a GTPase activating protein (GAP), needed to suppress RhoA activity. Our results reveal a matrix-specific pathway controlling migration involving a GEF/GAP interaction of β Pix with srGAP1 that is critical for maintaining suppressive crosstalk between Cdc42 and RhoA during 3D collagen migration.

Distinct biological responses of cells to interactions with different ECM proteins is necessary for efficient tissue development and wound repair, and is often deregulated in cancer⁶⁻⁹. Integrin binding to ECM proteins triggers selective activation of Rho GTPases, which induce cell polarization, cytoskeletal rearrangements, and contractile responses required for efficient migration in different microenvironments¹⁰⁻¹². However, a fundamental unanswered question is how specific Rho GTPase signaling pathways governing migration are regulated differentially by specific ECM proteins. These GTPases are regulated by GEFs, which activate them by facilitating the exchange of GDP- for GTP¹³. We hypothesized that adhesion to specific ECM molecules, such as collagen and fibronectin, would trigger differential GEF activation to regulate cell migratory responses.

Users may view, print, copy, and download text and data-mine the content in such documents, for the purposes of academic research, subject always to the full Conditions of use:http://www.nature.com/authors/editorial_policies/license.html#terms

Correspondence to Matthew L. Kutys: kutysml@mail.nih.gov; or Kenneth M. Yamada: kyamada@mail.nih.gov National Institutes of Health National Institute of Dental and Craniofacial Research Building 30, Room 426 30 Convent Dr MSC 4370 Bethesda, MD 20892-4370 Phone: (301) 496-9124 Fax: (301) 402-0897.

AUTHOR CONTRIBUTIONS

M.K. designed and carried out experiments. M.K. and K.Y. wrote the manuscript. K.Y. directed the project.

Nucleotide-free, dominant-negative Rho GTPase mutants can be used for affinity-isolation of activated GEFs^{14, 15}. We initially focused on GEFs for Rac1 because of its well-established role in driving 2D and 3D motility through coordination of lamellipodial dynamics¹⁶. In an ECM-based screen, we identified active GEFs binding to recombinant RacG15A, a Rac1 nucleotide-free mutant, from lysates of primary human foreskin fibroblasts (HFFs) undergoing steady-state migration in collagen, fibronectin, or ECM-free environments. We utilized an unbiased screening approach^{14, 15} for identification of active GEFs in cells migrating in specific ECM environments by identifying protein bands in Coomassie-stained polyacrylamide gels that bound selectively to RacG15A in different ECM environments (Supplementary Fig. 1a). Multiple GEFs were isolated that showed increased activity on both fibronectin and collagen (Fig. 1a, Supplementary Fig. 1b), but the Rac1/Cdc42 GEF β Pix was activated robustly and specifically only during migration on collagen (Fig. 1b). β Pix exists at multiple subcellular sites, including focal adhesions and plasma membrane, consistent with differential functions¹⁷⁻¹⁹. We therefore examined for altered localization of β Pix during fibroblast migration on fibronectin versus fibrillar collagen. As expected, both immunofluorescence staining for endogenous β Pix and live-cell imaging of GFP- β Pix showed strong localization to focal adhesions during migration on fibronectin and 3D cell-derived matrix (CDM), where the primary ECM ligand is fibronectin²⁰ (Fig. 1c, Supplementary Fig. 1d-g). Surprisingly, we found a dramatic decrease in both endogenous and GFP- β Pix focal adhesion localization in fibroblasts migrating on both fibrillar collagen and 3D collagen (Fig. 1c, Supplementary Fig. 1d-g). Subcellular fractionation revealed that on fibrillar collagen, endogenous β Pix transitioned from detergent-soluble to -insoluble fractions (Fig. 1d), and live cell GFP- β Pix imaging displayed a patchwork localization on ventral cell membranes in amorphous, persistent aggregates of variable size that, while polarized to leading-edge protrusions, did not co-localize with paxillin (Supplementary Fig. 1g). These data demonstrate that the intracellular location of β Pix changes dramatically when cells migrate on collagen compared to fibronectin, supporting the existence of ECM-specific functions observed in the initial GEF screen.

We next tested whether β Pix has collagen-specific functions in cell morphology or migration. Lentiviral-mediated knockdown of β Pix in HFFs with two independent shRNA hairpins (Supplementary Fig. 1c) revealed that loss of β Pix resulted in cells with rounded morphology, inability to spread in 3D collagen matrices, and severe motility defects in 3D collagen; in contrast, there were no effects in CDM (Fig. 1e,f,i, Supplementary Movie 1). This phenotype was characterized by rapid, transient formation of spatially deregulated cell protrusions (Fig. 1f arrowheads, Fig. 1j) with minimal cell motility compared to nonspecific shRNA control cells in 3D collagen (Fig. 1g,k). In addition to three fibroblast lines (HFF, BR5, BJ5ta), this collagen-specific β Pix knockdown phenotype was observed in additional cell types including primary human osteoblasts, aortic smooth muscle cells, umbilical vein endothelial cells, and invasive epithelial-derived adenocarcinoma cells (Supplementary Fig. 1h-j). Loss of β Pix led to severe morphological and migratory defects specific to collagen environments in all cell types we tested (Supplementary Fig. 1k,l). Although no obvious alterations were observed in focal adhesions, actin cytoskeleton, or microtubules (Supplementary Fig. 2a), the collagen fibers adjacent to β Pix knockdown cells were remodeled robustly by contraction/compaction that often tore holes in the collagen matrix

(Fig. 1h, asterisks). Interestingly, even high concentrations of globular collagen could not fully recapitulate the characteristic β Pix knockdown phenotype in 3D collagen or on thin, fibrillar collagen substrates (Supplementary Movie 2, Fig. 1k). These fibrillar collagen substrates are thin for improved optical imaging, but they retain the fibrillar structure of 3D collagen gels and underscore the importance of using more-physiological polymerized collagen fibers rather than globular monomeric collagen. Expression of shRNA-resistant GFP- β Pix at near-endogenous levels in cells with knockdown of endogenous β Pix rescued both morphological and migratory defects (Supplementary Figs. 2b,c, 4d). Thus, β Pix has a critical, matrix-specific role in cell migration in fibrillar collagen environments, with knockdown leading to hyper-protrusive, hyper-contractile cells incapable of efficient migration.

Because β Pix is a dual specificity GEF²¹, we tested its effects on Rac1 and Cdc42 activity during migration in fibrillar collagen microenvironments. β Pix bound specifically to the nucleotide-free mutant of Rac1, with no binding to recombinant wild-type or a constitutively active mutant (Supplementary Fig. 2j). Consistent with its reported function as a Rac1/Cdc42 GEF²¹, β Pix knockdown resulted in collagen-specific decreases in both Rac1 (~20%) and Cdc42 (~30%) activities (Fig. 2a,b). Similar to RacG15A, β Pix differentially bound to recombinant Cdc42G15A (Fig. 2c). It displayed increased but partial co-localization with Cdc42 in leading edge protrusions (Supplementary Fig. 3a) during migration on fibrillar collagen, but not fibronectin. Independent single-siRNA knockdowns for each protein were performed to determine whether depletion of Rac1 or Cdc42 would recapitulate the β Pix knockdown phenotype in 3D collagen (Fig. 2d, Supplementary Fig. 2d-i). Surprisingly, we found that knockdown of Cdc42, but not Rac1, fully mimicked β Pix knockdown in 3D collagen. While Rac1 knockdown cells mirrored nonspecific siRNA controls, Cdc42 knockdowns displayed the rounded, hyper-contractile morphology observed with loss of β Pix (Fig. 2e,f,h). We used multiple Rac-isoform knockdowns to rule out compensatory roles of other Rac isoforms (Rac2, Rac3) after Rac1 knockdown (Supplementary Fig. 2d-i), indicating that the collagen- β Pix knockdown phenotype was due to loss of Cdc42 activity, but not Rac1. This deregulated protrusive behavior of Cdc42 or β Pix-depleted cells was accompanied by defective migration in both 3D and thin fibrillar collagen environments (Supplementary Movie 3, Fig. 2i), along with physical tearing of holes in the surrounding matrix. These findings are consistent with a report that loss of Cdc42 in 3D microenvironments leads to temporally and spatially deregulated protrusions and impaired leading edge coordination²². We therefore investigated whether β Pix regulates the localization and activity of Cdc42 under different ECM conditions. Imaging a single-chain Cdc42 biosensor based on intramolecular fluorescence resonance energy transfer (FRET)²³ revealed that on fibronectin, Cdc42 activity remains polarized toward the leading edge of migrating cells expressing either nonspecific or β Pix shRNA (Fig. 2g). On collagen, Cdc42 activity was also polarized to the leading edge in the same regions where β Pix was found to uniquely localize on the membrane. In contrast, β Pix knockdown on fibrillar collagen led to a loss of this polarization and decreased overall Cdc42 activity (Fig. 2g, Supplementary Fig. 2l,m). Additionally, we observed similar collagen-specific decreases in Cdc42 FRET and loss of FRET polarization in 3D collagen, but not 3D cell-derived matrix (Supplementary

Fig. 2k), further establishing that β Pix acts through Cdc42, but not Rac1, to coordinate migration in fibrillar collagen environments.

Because of the strong collagen contraction phenotype associated with loss of β Pix, we speculated that β Pix/Cdc42 knockdown might increase RhoA activity during migration in fibrillar collagen environments. We assayed intracellular RhoA activity during fibronectin or fibrillar collagen migration in the presence and absence of β Pix. Knockdown of β Pix resulted in 40-60% increased intracellular RhoA activity in fibrillar collagen, but not fibronectin (Fig. 3a,b), with similar increases during 3D collagen migration (Supplementary Fig. 3e). Importantly, knockdown of Cdc42, but not Rac1, also increased intracellular RhoA activity levels on fibrillar collagen (Fig. 3c,d). We next used a single chain RhoA FRET biosensor^{23, 24} to determine RhoA activity and localization during live-cell migration. Cells migrating on fibronectin displayed a gradient of RhoA activity that was highest at the rear of the cell and decreased toward the leading edge (Fig. 3e). This localization pattern was also observed during migration on fibrillar collagen; however, after β Pix knockdown, we observed a striking loss of this RhoA gradient with a general elevation of RhoA activity (Fig. 3e-g). Again, the loss of front-back RhoA FRET segregation and elevation in activity was observed in 3D collagen, but not 3D cell-derived matrix (Supplementary Fig. 3b), confirming the suppressive crosstalk mechanism between β Pix/Cdc42 and RhoA in collagen microenvironments. We examined whether artificial increases in RhoA activity alone could mimic β Pix knockdown in 3D collagen. Low-level overexpression of constitutively active RhoAQ63L, as determined by fluorescence intensity, not only mimicked the rounded morphology (Fig. 3h,i) and robust collagen contraction (Supplementary Fig. 3c), but notably also the deregulated, hyper-protrusive behavior (Fig. 3h,j); expressing RhoAQ63L at comparable levels in HFFs migrating in cell-derived matrix did not perturb morphology or lead to hyper-protrusive behavior. Migration in fibrillar collagen environments (Supplementary Movie 4, Fig. 3k) was also significantly inhibited with low RhoAQ63L expression. Finally, to test directly whether inhibiting RhoA could partially rescue the β Pix knockdown phenotype, we treated β Pix knockdown cells with the RhoA inhibitor C3 transferase, or with blebbistatin to inhibit the RhoA effector myosin II. Treating β Pix knockdown cells in 3D collagen with C3 transferase significantly rescued both morphology and migration, while blebbistatin rescued the morphology with slight increases in motility (Fig. 3l, Supplementary Fig. 3d). We conclude that β Pix acts through Cdc42 to suppress and localize RhoA activity during migration in fibrillar collagen environments.

To address mechanistically how β Pix acts through Cdc42 to suppress RhoA, we utilized GFP- β Pix knockdown/rescue fibroblasts to isolate the proteins that bound differentially to β Pix from cells undergoing migration on fibronectin versus fibrillar collagen (Supplementary Fig. 2b, 4a). Immunoblotting for known binding partners such as Pak1 revealed decreased association on collagen compared to fibronectin, confirming differential binding to β Pix (Fig. 4b). Unexpectedly, mass spectrometry analysis of a strong ~130 kDa band revealed a collagen-specific association between β Pix and the RhoGAP srGAP1 in both HFFs (Fig. 4a) and MDA-MB-231 cells (Supplementary Fig. 4h). GAPs inactivate Rho proteins by stimulating their intrinsic GTPase activity and are critical elements in inhibitory Rho family crosstalk^{4, 25, 26}. Depending on the context, srGAP1 can promote the GTP

hydrolysis of RhoA, Cdc42, or Rac1²⁷, and overexpression of srGAP1 can suppress protrusive plasma membrane dynamics²⁸.

To test the role of srGAP1 in the β Pix/Cdc42 collagen pathway, we performed RNAi knockdown (Supplementary Fig. 3f) and assayed for intracellular RhoA activity. Intracellular RhoA activity levels increased significantly after loss of srGAP1 during fibrillar collagen migration but not on fibronectin (Fig. 4c,d), with no change in Rac1 activity during migration of collagen (Supplementary Fig. 3h). Knockdown of srGAP1 fully mimicked the phenotype characteristic of β Pix and Cdc42 knockdown in 3D collagen (Supplementary Movie 5), i.e., rounded cells with hyperactive, de-localized protrusions, loss of persistent motility, and increased contraction of adjacent collagen matrix (Fig. 4e-g, Supplementary Fig. 3f,g). This result identifies an interaction between a GEF-GAP pair that mediates Cdc42 and RhoA crosstalk. This mechanism involving β Pix/Cdc42/srGAP1 serves to locally suppress RhoA activity and promote efficient cell migration in fibrillar collagen environments.

Having identified a collagen-specific role for β Pix, we searched for mechanisms regulating β Pix in different matrix conditions. We first tested for integrin-specific regulation of β Pix using certain anti-integrin monoclonal antibodies that can mimic full integrin ligation and adhesive function²⁹. Using loss of focal adhesion localization as a read-out of signaling to β Pix (as observed on fibrillar collagen, Fig. 1c), we assayed the localization of GFP- β Pix in knockdown/rescue cells migrating on substrates coated with antibodies toward β 1, α 5, and α 2 integrin. GFP- β Pix strongly co-localized to focal adhesions stained for paxillin on glass or substrates targeting β 1 and α 5 integrin (Fig. 5a). However, on substrates targeting α 2 integrin, GFP- β Pix localization to focal adhesions was greatly diminished, even though paxillin-containing focal adhesions were formed normally. Conversely, treatment of cells migrating in 3D collagen with inhibitory antibodies against specific integrins confirmed specificity for the α 2 β 1 integrin by blocking migration (Supplemental Fig. 4b). Thus, the α 2 subunit of α 2 β 1 integrin is important for mediating β Pix function during migration in fibrillar collagen environments.

Regulation of β Pix function has been ascribed to multiple phosphorylation sites on the protein³⁰. To test whether specific phosphorylation sites were important for β Pix function during collagen migration, we performed phosphoproteomics on GFP- β Pix isolated from knockdown/rescue cells during migration on fibronectin versus fibrillar collagen (Supplemental Fig. 4c). We identified a selective loss of threonine phosphopeptides at T526 only during fibrillar collagen migration, and confirmed by western blotting decreased threonine phosphorylation on β Pix during migration on fibrillar collagen compared to fibronectin (Fig. 5b). This matrix-specific threonine phosphorylation was lost after mutating T526 to alanine (T526A) (Fig. 5b) in GFP- β Pix knockdown/rescue HFFs, confirming that the phosphorylation of T526 is altered during migration on fibronectin versus fibrillar collagen. T526 phosphorylation is crucial for contextual Rac1 activation³¹ and β Pix translocation to focal complexes³², consistent with our findings of loss of these actions during migration on collagen. To test whether absence of T526 phosphorylation is important for β Pix function in collagen, we generated stable β Pix knockdown/rescue fibroblasts with either phospho-dead (KDR-T526A) or phospho-mimetic (KDR-T526E) mutations, with the

hypothesis that mimicking phosphorylation at T526 would prevent morphological and migratory rescue. As predicted, re-expression of β Pix with a phospho-mimetic mutation at T526 could not rescue the spreading and collagen contraction/remodeling defects of β Pix knockdown (Fig. 5c, Supplementary Fig. 4d), whereas T526A β Pix-expressing cells were fully rescued morphologically. Additionally, T526E cells could not rescue cell migration in 3D collagen gels, while T526A expression mirrored migratory velocities of rescued KDR-WT cells (Fig. 5d). Similar morphological and migratory phenotypes were observed for β Pix knockdown/rescue phosphovariants in MDA-MB-231 adenocarcinoma cells in 3D collagen (Supplementary Fig. 4e-g). Mechanistically, immunoprecipitation of GFP- β Pix knockdown/rescue phosphovariants during migration on fibrillar collagen revealed that the β Pix phosphorylation mimetic (T526E) had decreased association with srGAP1, but not Cdc42 (Fig. 5e). These data indicate that loss of phosphorylation at T526 on β Pix is essential for its association with srGAP1 during fibrillar collagen migration.

To investigate the upstream regulation of T526 on β Pix during migration in fibrillar collagen, we again utilized our GFP- β Pix knockdown/rescue fibroblasts to isolate collagen-specific β Pix-binding proteins. We identified a collagen-specific interaction between β Pix and protein phosphatase 2A (PP2A) through the regulatory subunit A α isoform (PPP2R1A) in both HFFs (Fig. 5f) and MDA-MB-231 cells (Supplementary Fig. 4h). PP2A can be activated specifically during migration in 3D collagen, but not fibronectin, through $\alpha_2\beta_1$ integrin³³. To assess the role of PP2A in the β Pix-collagen pathway, we utilized both siRNA toward PPP2R1A and okadaic acid, a potent, specific inhibitor of PP2A activity³³. Knocking down PPP2R1A with two independent siRNAs (Supplementary Fig. 5a,c-e) or treating HFFs with 1 nM okadaic acid (Supplementary Fig. 5b,f) revealed the same collagen-specific morphological and migratory defects mirroring β Pix knockdown. Moreover, treatment of GFP- β Pix knockdown/rescue cells migrating on fibrillar collagen with siRNA (Fig. 5g) or okadaic acid (Supplementary Fig. 5g) led to a direct increase in threonine phosphorylation on β Pix in comparison to controls. To functionally link the association of β Pix with PPP2R1A to reduced T526 phosphorylation, we performed loss-of-function experiments by treating knockdown/rescue wild type and T526A fibroblasts with PPP2R1A siRNA and assaying cell morphology and migration in 3D collagen. While knocking down PPP2R1A led to severe morphological and migratory defects in β Pix KDR-WT fibroblasts, β Pix KDR-T526A fibroblasts rescued the morphological phenotype and partially rescued the migratory defect resulting from PPP2R1A knockdown in 3D collagen (Supplementary Fig. 5h-j). These data indicate that PP2A is critical for regulating the absence of phosphorylation at T526 on β Pix during migration in fibrillar collagen environments.

Our findings establish that ECM-dependent regulation of a specific GEF is a fundamental mechanism governing migration in different microenvironments. We demonstrate that β Pix is critical for efficient migration in fibrillar collagen environments by restraining RhoA signaling (Fig. 5h). Interestingly, this suppression occurs through a mechanism of Rho GTPase crosstalk between Cdc42 and RhoA that is regulated by a collagen-specific functional interaction between the GEF/GAP pair, β Pix and srGAP1. Additionally, our model suggests that binding of $\alpha_2\beta_1$ to fibrillar collagen leads, through PP2A, to loss of phosphorylation at T526 on β Pix and promotes association with srGAP1. T526 is a

phosphorylation site for Pak1 and PKA, and is implicated in Pak2 signaling^{32, 34}. Our observation of decreased association between β Pix and Pak1 during migration in fibrillar collagen (Fig. 4b) may suggest that decreased activity of a kinase phosphorylating β Pix could also contribute to regulating T526 phosphorylation in response to fibrillar collagen.

Although there are many complex interactions and crosstalk occurring at the leading edge of cells during migration, the β Pix/srGAP1 complex provides an elegant mechanism for restricting RhoA and concentrating Cdc42 activity toward the leading edge in collagen microenvironments. We speculate that this and other potential specific GEF/GAP interactions could provide local contextual regulation in other ECM microenvironments that affects differentiation, morphogenesis, and tumor progression through RhoA signaling^{7, 35-38}. Our findings provide a mechanistic link between an external stimulus from collagen to regulation of Cdc42 and RhoA signaling during 3D cell migration.

METHODS

Cell lines and reagents

Primary human foreskin fibroblasts (HFFs), immortalized human fibroblasts (BJ5Ta and BR5, ATCC), human adenocarcinoma line MDA-MB-231, primary human osteoblasts (NhOst, Lonza), and HEK 293FT cells were cultured in phenol red-free DMEM (Hyclone) supplemented with 10% fetal bovine serum (Hyclone), 100 U/ml penicillin, 100 μ g/ml streptomycin (Invitrogen), and 2 mM L-glutamine (Invitrogen) at 37°C in 10% CO₂ in a humidified incubator. Human umbilical vein endothelial cells (HUVECs) and human aortic smooth muscle cells (AOSMCs, Lonza) were cultured in phenol red-free DMEM (Hyclone) supplemented with 5% fetal bovine serum (Hyclone), insulin, hFGF, and hEGF (Lonza, SMGM-2 BulletKit) at 37°C in 5% CO₂. The following reagents were used in this study: rhodamine- and Alexa488-phalloidin (Invitrogen), cell-permeable C3 transferase (Cytoskeleton), blebbistatin and okadaic acid (EMD), and GFP-TRAP GFP-binding protein (Chromotek). GFP-RhoQ63L was transfected into cells with the Nucleofector system (Lonza) using the NDHF kit (Lonza) according to the manufacturer's instructions. Equal concentrations of the DMSO vehicle were used as controls for drug studies.

Antibodies

The anti- β Pix antibody (07-1450, 1:1000), anti-GFP (3F8.2, 1:1000), anti-PAK1 (EP656Y, 1:500), anti-Rac3 (07-2151, 1:500), anti-Rac2 (07-604, 1:500), and anti-PPPR2A1 (07-250, 1:1000) were from Millipore. Anti-Rac1 (102, 1:1000), anti-Cdc42 (44, 1:500), and anti-paxillin (349, 1:100) were from BD Biosciences. Anti-RhoA antibody (ab54835, 1:1000) and anti-beta tubulin (ab6046, 1:5000) were from Abcam. Anti-p-Threonine (42H4, 1:500) antibody was from Cell Signaling. Rabbit polyclonal antibody (5836, 1:2500) toward fibronectin was produced in-house. Anti-GAPDH (6c5, 1:5000) was from Fitzgerald and anti-actin (AC-40, 1:1000) was from Sigma. Anti-srGAP1 (286A, 1:500) was from Bethyl laboratories, and anti-SmgGDS was from Novus Biologicals.

RNA-mediated interference

Individual ON-TARGETplus siRNAs toward β Pix, srGAP1, Rac3, Rac2, and PPP2R1A (Dharmacon-Thermo Scientific) and previously validated⁹ Rho GTPase siRNAs toward Rac1 and Cdc42 (Silencer Select, Invitrogen) were used for protein knockdown. All protein knockdowns were conducted with at least two independent RNAi sequences. For specific sequence information and labels see Supplementary Table 1. siRNAs were transfected into cells using Lipofectamine 2000 (Invitrogen) as previously described^{9,16}.

Lentiviral-mediated generation of stable fibroblast lines

Stable β Pix knockdown and knockdown-rescue cells lines in primary HFFs were generated using the pLL 3.7 lentiviral packing system (11795, Addgene) as described previously³⁹. Two independent shRNA hairpins targeting β Pix regions: shRNA#2: 5'-GGAAGAAGATGCTCAGATT-3' and shRNA#4: 5'-GTAGTAAGAGCAAAGTTTA-3', along with a nonspecific control, 5'-GGAATCTCATTCGATGCAT-3' were cloned into the pLL3.7 lentiviral vector. For knockdown-rescue constructs, β Pix cDNA (Origene) was cloned into pLL3.7 at the NheI-EcoRI restriction sites, creating C-terminal tagged GFP- β Pix. The QuikChange Site-Directed Mutagenesis kit (Stratagene) was used to create three nucleotide substitutions that did not perturb the amino acid sequence in β Pix to generate a shRNA-resistant construct. Additionally, similar mutagenesis techniques were used to introduce phospho-mimetic (KDR-T526E) and phospho-dead (KDR-T526A) mutations into β Pix cDNA in the pLL 3.7 knockdown-rescue construct. GFP or mCherry-positive cells were isolated by fluorescence-activated cell sorting (BD FACS ARIA).

Purification of recombinant proteins

RacG15A and Cdc42G15A were cloned into pGEX4T-1 using the EcoRI-BamHI restriction sites. pGEX4T-1 constructs containing the Rho-binding domain (3x RBD) of Rhotekin cDNA was a kind gift from Silvio Gutkind (NIDCR) and the p21-binding domain of Pak1 (PBD) was from Addgene (Plasmid 12217). Briefly, expression of the GST fusion proteins in *BL21 Escherichia coli* was induced with 200 μ M isopropyl- β -D-thiogalactoside (IPTG) for 12-16 hours at room temperature. Bacterial cells were lysed in buffer containing 20 mM HEPES pH 7.6, 1% Triton X-100, 150 mM NaCl, 5 mM MgCl₂, 1 mM dithiothreitol, protease and phosphatase inhibitor cocktails (Roche), and the proteins were purified by incubation with glutathione-Sepharose 4B beads (GE Healthcare) at 4 °C.

Mass spectrometry analysis

Single, excised Coomassie stained bands for protein identification and phosphorylation analysis were analyzed by MS Bioworks as follows. In-gel digestion was performed using a ProGest robot (DigiLab). Gel bands were washed with 25 mM ammonium bicarbonate followed by acetonitrile, reduced with 10 mM dithiothreitol at 60°C followed by alkylation with 50 mM iodoacetamide at room temperature, digested with trypsin (Worthington) at 37°C for 4h, and quenched with formic acid, and the supernatant was analyzed directly without further processing. Each digested sample was analyzed by nano LC/MS/MS with a Waters NanoAcquity HPLC system interfaced to a ThermoFisher Q Exactive mass spectrometer. 30 μ L of sample was loaded on a trapping column and eluted over a 75 μ m

analytical column at 350 nL/min; both columns were packed with Jupiter Proteo resin (Phenomenex). The mass spectrometer was operated in data-dependent mode, with MS and MS/MS performed in the Orbitrap at 70,000 and 17,500 FWHM resolution, respectively. The fifteen most abundant ions were selected for MS/MS. LC/MS/MS data were analyzed using the MASCOT algorithm, with trypsin specified as the digestion enzyme (two max missed cleavages) and all data searched against the SwissProt Human database (forward and reverse appended with common contaminant proteins). Carbamidomethylation (C) was set as fixed modification. For protein identification, Oxidation (M), Acetyl (N-term), Pyro-Glu (N-term Q), Deamidation (N,Q) were selected as variable. For phosphoanalysis, the same modifications were variable, in addition to Phospho (S-T-Y). Peptide mass tolerances were set to 10 ppm and fragment mass tolerance set to ± 0.015 Da. Mascot DAT files were parsed into the Scaffold software for validation, filtering and to create a non-redundant list per sample. The data were filtered using a minimum protein value of 80%, and a minimum peptide value of 50% (Prophet scores).

GEF activity and GTPase activity affinity assays

GST-RacG15A active GEF-pulldown experiments were carried out as described previously^{14,15}. Dishes were coated with 10 $\mu\text{g/ml}$ human plasma-derived fibronectin or 50 $\mu\text{g/ml}$ rat tail type I collagen overnight at 4°C. HFFs were serum starved for 2 hours prior to plating, then plated in serum-free DMEM and allowed to reach steady-state migration over 12-16 hours. Cells were lysed in 20 mM HEPES pH 7.6, 1% Triton X-100, 150 mM NaCl, 5 mM MgCl₂, 1 mM dithiothreitol, protease and phosphatase inhibitor cocktails (Roche) and sonicated at 3W on ice for five seconds at 4°C using a Misonix Microson XL sonicator. Lysates adjusted to equal quantities and concentration of protein were incubated with 25 μg of purified GST-RacG15A or GST-Cdc42G15A for 1 hour at 4°C. Samples were washed in lysis buffer (3 times for Western blotting or 5 times for mass spectrometry) and analyzed by SDS-PAGE using Novex® Tris-Glycine 4-12% polyacrylamide gels (Invitrogen). For identification of the GEFs bound to RacG15A by mass spectrometry, SDS-PAGE gels were Coomassie-stained with GelCode Blue Stain Reagent (Pierce). Bands of interest were extracted and identified using nano LC/MS/MS (MS Bioworks). For active RhoA, Cdc42 and Rac1-pulldowns, plates and cells were prepared as indicated above. Fibroblasts that were cultured overnight in complete media (RhoA) or serum-free media (Rac1, Cdc42) were lysed in 50 mM Tris pH 7.6, 200 mM NaCl, 1% Triton X-100, 0.5% deoxycholate, 5 mM MgCl₂, and protease and phosphatase inhibitor cocktails, sonicated at 3W on ice for five seconds, and clarified at 12,000 \times g for 5 minutes. Lysates were equalized for protein content and volume and rotated at 4°C for 1 hour with either 20 μg GST-RBD or 30 μg GST-PBD. Bead pellets were washed three times with lysis buffer and analyzed by SDS-PAGE as described above. Polyacrylamide gels were transferred to nitrocellulose membranes using the semi-dry iBlot® transfer system (Invitrogen). Membranes were blocked with Odyssey blocking buffer (LI-COR) for one hour at room temperature. Primary antibodies were incubated with membranes in Odyssey blocking buffer containing 0.1% Tween-20 overnight at 4°C. Membranes were washed with TBS containing 0.1% Tween-20 (TBST) three times over 30 minutes. IRDye-conjugated anti-mouse and rabbit secondary antibodies (1:20,000) (LI-COR) were incubated in Odyssey blocking buffer containing 0.1% Tween-20 for 30 minutes at room temperature. Membranes were then washed with TBS containing 0.1%

Tween-20 (TBST) three times over 30 minutes. All Western blots were imaged and quantified using the Odyssey imaging system through the analyze module (LI-COR). Intensity values were normalized to load control (tubulin or GAPDH).

Membrane fractionation and immunoprecipitation

For Triton X-100 membrane fractionation, cells cultured on matrix overnight in complete media were lysed in 50 mM Tris pH 7.6, 150 mM NaCl, 1% Triton X-100, and protease and phosphatase inhibitor cocktails. Lysates were vortexed and incubated by end-over-end rotation for 20 minutes at 4°C. Cell lysates were fractionated by centrifuging at $15,500 \times g$ for 15 minutes. The resulting pellets (insoluble fraction) were washed three times with lysis buffer and then denatured in 2x Novex sample buffer (Invitrogen) containing 100 μ M dithiothreitol for 5 minutes at 95°C. Pellets were compared to supernatant (soluble fraction) by SDS-PAGE using Novex® Tris-Glycine 4-12% polyacrylamide gels (Invitrogen). For immunoprecipitation of GFP- β Pix from fibrillar collagen environments, cells cultured on matrix overnight in complete media were lysed in 50 mM Tris pH 7.6, 200 mM NaCl, 1% Triton X-100, 0.5% deoxycholate, 5 mM $MgCl_2$, and protease and phosphatase inhibitor cocktails (Roche), homogenized using 200-1000 μ l positive displacement pipets (Anachem), sonicated at 3W on ice for three seconds, and incubated for 7 minutes with end-over-end rotation at 4°C. Lysates were clarified by centrifugation at $12,000 \times g$, equalized for protein content and volume, and incubated for 1 hour with 30 μ l of GFP-TRAP (Chromotek) conjugated to magnetic beads at 4°C with end-over-end rotation. For mass spectrometry analysis, beads were washed five times with lysis buffer and analyzed by SDS-PAGE and Coomassie blue staining. For the identification of srGAP1, excised gel bands were analyzed using nano LC/MS/MS (MS Bioworks).

Generation of cell-derived matrices (CDMs)

CDMs were prepared from HFFs as described previously⁹. MatTek dishes were coated with 0.2% gelatin for 1 h at 37°C, treated with 1% glutaraldehyde for 30 min at RT, and incubated with DME for 30 min at RT. Three washes with Dulbecco's PBS with calcium and magnesium (PBS+) followed each treatment. 4×10^5 HFFs were plated per MatTek dish, which were maintained for 10 d, adding fresh media with 50 μ g/ml ascorbic acid every other day. The cells were removed from the CDM with extraction buffer (20 mM NH_4OH and 0.5% Triton X-100 in PBS+) for 5 min at RT and washed with PBS+. The cell-free CDM was treated with 10 U/ml DNase (Roche) for 30 min at 37°C, washed with Dulbecco's PBS without calcium and magnesium (PBS), and stored at 4°C in PBS with 100 U/ml penicillin and 100 μ g/ml streptomycin.

Generation of fibrillar collagen matrices and time lapse microscopy

2 mg/ml fibrillar collagen gel solutions were prepared by mixing rat tail type I collagen with 10x reconstitution buffer (0.26 M $NaHCO_3$ and 0.2 M HEPES) and 10X DME (Sigma), adjusting the pH to 7.4 with 1M NaOH, and then diluting to 2 mg/ml with PBS+ To generate thin fibrillar collagen substrates, 30 μ l of solution was spread on a 20 mm MatTek dish and allowed to polymerize for 1 hour at room temperature. Using these substrates for biochemical assays facilitated cellular extraction and minimized collagen contamination in comparison to 3D collagen. Additionally, these substrates minimized light scatter during

imaging, while still providing the fibrillar collagen substrate required for the β Pix knockdown phenotype. Fibroblasts were plated in complete medium overnight and assayed for motility the following day. For 3D collagen gels, cells were resuspended in PBS+ and mixed with the prepared collagen mixture. The collagen-cell mixture was spread on MatTek dishes and allowed to polymerize at room temperature for 1 hour. Complete medium was added to the gels, and the cells were assayed for motility the next day. For phase contrast microscopy timelapse imaging of fibroblasts in different matrix environments, complete medium was added prior to image acquisition. For inhibitor treatments, vehicle control or inhibitors were incubated with cells for 4-6 hours before beginning the timelapse. Random cell migration was imaged for 24 hours in 37°C, 10% CO₂ environmental chambers. Timelapse videos were recorded on a microscope (Axiovert 135TV; Carl Zeiss, Inc.) fitted with a motorized xy- and z-stage focus drive (Ludl Electronic Products Ltd.) using an enhanced contrast Plan-Neofluar 10× 0.3 NA or a long-working distance Plan-Neofluar Korr 20× 0.4 NA objective (Carl Zeiss, Inc.). Images were acquired with a charge-coupled device camera (ORCA II ER; Hamamatsu Photonics). Microscopy images were adjusted for brightness and contrast and cells were tracked manually using MetaMorph software.

Live cell fluorescence and FRET imaging

Fibroblasts were imaged with a modified Yokogawa spinning-disk confocal scan head (CSU-21: modified by Spectral Applied Research Inc.) attached to an automated Olympus IX-81 microscope using a 60X SAPO-Chromat silicone oil objective (N.A. 1.3). A custom laser launch equipped with 442 nm (40 mW: Melles Griot), 488 nm (150 mW: Coherent), 514 nm (150 mW: Coherent), 568 nm (100 mW: Coherent), and 642 nm (110 mW: Vortran) diode lasers supplied excitation wavelengths. A Gooch and Housego AOTF controlled shuttering and intensity for 488, 514, and 568 laser lines. 442 and 642 lines were shuttered and intensity controlled via TTL and direct voltage steps, respectively. The primary dichroics (442/568/647 and 405/488/568/647) were from Semrock. Images were captured using a backthinned EM CCD camera in 16-bit format using the 10 MHz digitization setting (Roper Scientific).

mCherry was cloned into pLL3.7 in place of GFP to allow FRET compatibility. mCherry- β Pix knockdown fibroblasts were generated with the shRNA#2 hairpin. The binding of active Cdc42 or RhoA was detected by imaging the FRET-dependent, intramolecular emission fluorophore (YPet) from YPet-PAK-EV-Cdc42-CFP or YPet-RBD-EV-RhoA-CFP²⁴ (kind gifts from M. Matsuda). Fibroblasts were transfected as indicated using the Nucleofector system (Amaxa) according to the manufacturer's instructions. The next day, cells were trypsinized and plated onto fibronectin or fibrillar collagen matrices in complete media and allowed to adhere overnight. Cells were imaged the following morning in 5% fetal bovine serum, phenol-red free DMEM with 10 units/ml Oxyrase. Optimal FRET acquisition settings were determined for the Olympus IX-81 spinning disc microscope and strictly maintained during all subsequent FRET imaging; intensity levels of biosensor expression were similarly carefully controlled and maintained between selected cells. Ratio FRET images were obtained as previously described⁴⁰. Images of CFP and YPet were obtained for each z-plane under 442 nm illumination. Maximum projections of confocal z-stacks were generated using MetaMorph software. Images were first background subtracted

and a binary mask was applied by thresholding to the cytoplasmic mCherry-lentiviral marker to isolate the cellular signal. FRET ratio images were generated in MetaMorph using the arithmetic module, with a universally applied scaling factor of 1000. All resulting FRET images were processed with a 3x3 median filter to remove any hot pixels and presented in a pseudocolor map (MetaMorph). The same pseudocolor intensity scale was maintained for each ECM condition for the NS and β Pix shRNA conditions. Polarization index (PI) was calculated as previously described⁹ using the five highest points of FRET intensity per cell analyzed. A PI of 1 = forward polarization, 0 = nonpolarization (regions are uniformly distributed), and -1 = rearward polarization.

Immunofluorescence

For morphological analysis in 3D collagen or CDM and immunolocalization of Cdc42, cells cultured in complete medium were fixed with 4% paraformaldehyde in PBS+, permeabilized with 0.25% Triton X-100 in PBS+, and blocked with 1% BSA in PBS+. Rhodamine- or Alexa488-phalloidin and primary and secondary antibodies were applied in 1% BSA in PBS+ and samples were rinsed with PBS+ three times over 30 minutes between each treatment. Elliptical factor (E.F.) was calculated as the ratio of cell length to cell width at maximal points in 3D reconstructions using MetaMorph software. For localization analysis of β Pix to focal adhesions on fibrillar collagen, cells were fixed-permeabilized with 3% paraformaldehyde-0.5% Triton X-100 in PBS+ at 37°C followed by an additional fixation with 4% paraformaldehyde. Cells were blocked with 1% BSA in PBS+. Primary and secondary antibodies were applied in 1% BSA in PBS+ and rinsed three times over thirty minutes with PBS+ between each treatment. For all confocal microscope immunofluorescence analyses, cells were imaged with the same Yokogawa CSU-21/Olympus IX-81 spinning disc microscope listed for live-cell imaging with a 60X SAPO-Chromat silicone oil objective (N.A. 1.3) for morphological imaging and a Plan Apo N 150 \times 1.45 NA objective (TIRFM UIS2; Olympus) for β Pix localization imaging. For analysis of β Pix localization to focal adhesions after plating of cells on monoclonal integrin antibodies, dishes were coated with poly-L-lysine for ten minutes at room temperature, washed with PBS+, and incubated with each antibody in PBS+ for 1 hour at 37°C. Dishes were washed three times with PBS+ and blocked for a further hour at 37°C with 1% BSA. GFP- β Pix KDR (knockdown-rescue) cells were plated in complete media overnight. The next day, the same fix-permeabilization methodology was used as described above. Cells were imaged using TIRF microscopy, performed using an Olympus IX-71 microscope using a Plan Apo N 60 \times 1.45 NA objective (TIRFM UIS2; Olympus). Fluorescence images were adjusted for brightness and contrast using MetaMorph software.

Statistical analysis

When experiments involved only a single pair of conditions, statistical differences between the two sets of data were analyzed with a two-tailed, unpaired Student *t*-test with Prism5 (GraphPad Software). For data sets containing more than two samples, one-way ANOVA with a classical Bonferroni multiple comparisons post-test was used to determine adjusted *P* values. Sample sizes of sufficient power were chosen based on similar published research and were confirmed statistically by appropriate tests. Experiments were not randomized. However, the investigator was blinded during the assessment of key morphological and

migratory experiments involving β Pix, Cdc42, Rac1, and srGAP1 knockdowns under different matrix conditions by using randomization of data labels. Primary statistics source data for all main and supplementary figures are available in Supplementary Table 2. Statistically significant differences are reported at *, $P < 0.05$, **, $P < 0.01$ and ***, $P < 0.001$.

Supplementary Material

Refer to Web version on PubMed Central for supplementary material.

ACKNOWLEDGEMENTS

The authors would like to thank Will Daley, Ryan Petrie, and Duy Tran for critical reading of the manuscript. This study was supported by the Intramural Research Program of the National Institute of Dental and Craniofacial Research, NIH.

References

1. Friedl P, Wolf K. Plasticity of cell migration: a multiscale tuning model. *J Cell Biol.* 2010; 188:11–19. [PubMed: 19951899]
2. Arthur WT, Noren NK, Burridge K. Regulation of Rho family GTPases by cell-cell and cell-matrix adhesion. *Biol Res.* 2002; 35:239–246. [PubMed: 12415742]
3. Petrie RJ, Yamada KM. At the leading edge of three-dimensional cell migration. *J Cell Sci.* 2012; 125:5917–5926. [PubMed: 23378019]
4. Guilluy C, Garcia-Mata R, Burridge K. Rho protein crosstalk: another social network? *Trends Cell Biol.* 2011; 21:718–726. [PubMed: 21924908]
5. Doyle AD, Petrie RJ, Kutys ML, Yamada KM. Dimensions in cell migration. *Curr Opin Cell Biol.* 2013; 25:642–649. [PubMed: 23850350]
6. Frantz C, Stewart KM, Weaver VM. The extracellular matrix at a glance. *J Cell Sci.* 2010; 123:4195–4200. [PubMed: 21123617]
7. Provenzano PP, et al. Collagen reorganization at the tumor-stromal interface facilitates local invasion. *BMC Med.* 2006; 4:38. [PubMed: 17190588]
8. Daley WP, Yamada KM. ECM-modulated cellular dynamics as a driving force for tissue morphogenesis. *Curr Opin Genet Dev.* 2013; 23:408–414. [PubMed: 23849799]
9. Petrie RJ, Gavara N, Chadwick RS, Yamada KM. Nonpolarized signaling reveals two distinct modes of 3D cell migration. *J Cell Biol.* 2012; 197:439–455. [PubMed: 22547408]
10. Huttenlocher A, Horwitz AR. Integrins in cell migration. *Cold Spring Harb Perspect Biol.* 2011; 3:a005074. [PubMed: 21885598]
11. Petrie RJ, Doyle AD, Yamada KM. Random versus directionally persistent cell migration. *Nat Rev Mol Cell Biol.* 2009; 10:538–549. [PubMed: 19603038]
12. Raftopoulou M, Hall A. Cell migration: Rho GTPases lead the way. *Dev Biol.* 2004; 265:23–32. [PubMed: 14697350]
13. Bos JL, Rehmann H, Wittinghofer A. GEFs and GAPs: critical elements in the control of small G proteins. *Cell.* 2007; 129:865–877. [PubMed: 17540168]
14. Garcia-Mata R, et al. Analysis of activated GAPs and GEFs in cell lysates. *Methods Enzymol.* 2006; 406:425–437. [PubMed: 16472675]
15. Dubash AD, et al. A novel role for Lsc/p115 RhoGEF and LARG in regulating RhoA activity downstream of adhesion to fibronectin. *J Cell Sci.* 2007; 120:3989–3998. [PubMed: 17971419]
16. Pankov R, et al. A Rac switch regulates random versus directionally persistent cell migration. *J Cell Biol.* 2005; 170:793–802. [PubMed: 16129786]

17. Kuo JC, Han X, Hsiao CT, Yates JR 3rd, Waterman CM. Analysis of the myosin-II-responsive focal adhesion proteome reveals a role for beta-Pix in negative regulation of focal adhesion maturation. *Nat Cell Biol.* 2011; 13:383–393. [PubMed: 21423176]
18. Liu F, et al. Cadherins and Pak1 control contact inhibition of proliferation by Pak1-betaPIX-GIT complex-dependent regulation of cell-matrix signaling. *Mol Cell Biol.* 2010; 30:1971–1983. [PubMed: 20154149]
19. Cau J, Hall A. Cdc42 controls the polarity of the actin and microtubule cytoskeletons through two distinct signal transduction pathways. *J Cell Sci.* 2005; 118:2579–2587. [PubMed: 15928049]
20. Kutys ML, Doyle AD, Yamada KM. Regulation of cell adhesion and migration by cell-derived matrices. *Exp Cell Res.* 2013; 319:2434–2439. [PubMed: 23751565]
21. Manser E, et al. PAK kinases are directly coupled to the PIX family of nucleotide exchange factors. *Mol Cell.* 1998; 1:183–192. [PubMed: 9659915]
22. Lammermann T, et al. Cdc42-dependent leading edge coordination is essential for interstitial dendritic cell migration. *Blood.* 2009; 113:5703–5710. [PubMed: 19190242]
23. Komatsu N, et al. Development of an optimized backbone of FRET biosensors for kinases and GTPases. *Mol Biol Cell.* 2011; 22:4647–4656. [PubMed: 21976697]
24. Yoshizaki H, et al. Activity of Rho-family GTPases during cell division as visualized with FRET-based probes. *J Cell Biol.* 2003; 162:223–232. [PubMed: 12860967]
25. Ohta Y, Hartwig JH, Stossel TP. FilGAP, a Rho- and ROCK-regulated GAP for Rac binds filamin A to control actin remodelling. *Nat Cell Biol.* 2006; 8:803–814. [PubMed: 16862148]
26. Bustos RI, Forget MA, Settleman JE, Hansen SH. Coordination of Rho and Rac GTPase function via p190B RhoGAP. *Curr Biol.* 2008; 18:1606–1611. [PubMed: 18948007]
27. Wong K, et al. Signal transduction in neuronal migration: roles of GTPase activating proteins and the small GTPase Cdc42 in the Slit-Robo pathway. *Cell.* 2001; 107:209–221. [PubMed: 11672528]
28. Coutinho-Budd J, Ghukasyan V, Zylka MJ, Polleux F. The F-BAR domains from srGAP1, srGAP2 and srGAP3 regulate membrane deformation differently. *J Cell Sci.* 2012; 125:3390–3401. [PubMed: 22467852]
29. Miyamoto S, et al. Integrin function: molecular hierarchies of cytoskeletal and signaling molecules. *J Cell Biol.* 1995; 131:791–805. [PubMed: 7593197]
30. Mayhew MW, et al. Identification of phosphorylation sites in betaPIX and PAK1. *J Cell Sci.* 2007; 120:3911–3918. [PubMed: 17989089]
31. Shin EY, et al. Basic fibroblast growth factor stimulates activation of Rac1 through a p85 betaPIX phosphorylation-dependent pathway. *J Biol Chem.* 2004; 279:1994–2004. [PubMed: 14557270]
32. Chahdi A, Miller B, Sorokin A. Endothelin 1 induces beta 1Pix translocation and Cdc42 activation via protein kinase A-dependent pathway. *J Biol Chem.* 2005; 280:578–584. [PubMed: 15513924]
33. Ivaska J, et al. Integrin alpha 2 beta 1 promotes activation of protein phosphatase 2A and dephosphorylation of Akt and glycogen synthase kinase 3 beta. *Mol Cell Biol.* 2002; 22:1352–1359. [PubMed: 11839802]
34. Koh CG, Manser E, Zhao ZS, Ng CP, Lim L. Beta1PIX, the PAK-interacting exchange factor, requires localization via a coiled-coil region to promote microvillus-like structures and membrane ruffles. *J Cell Sci.* 2001; 114:4239–4251. [PubMed: 11739656]
35. Engler AJ, Sen S, Sweeney HL, Discher DE. Matrix elasticity directs stem cell lineage specification. *Cell.* 2006; 126:677–689. [PubMed: 16923388]
36. Provenzano PP, et al. Collagen density promotes mammary tumor initiation and progression. *BMC Med.* 2008; 6:11. [PubMed: 18442412]
37. Daley WP, et al. ROCK1-directed basement membrane positioning coordinates epithelial tissue polarity. *Development.* 2012; 139:411–422. [PubMed: 22186730]
38. Levental KR, et al. Matrix crosslinking forces tumor progression by enhancing integrin signaling. *Cell.* 2009; 139:891–906. [PubMed: 19931152]
39. Cai L, Marshall TW, Uetrecht AC, Schafer DA, Bear JE. Coronin 1B coordinates Arp2/3 complex and cofilin activities at the leading edge. *Cell.* 2007; 128:915–929. [PubMed: 17350576]

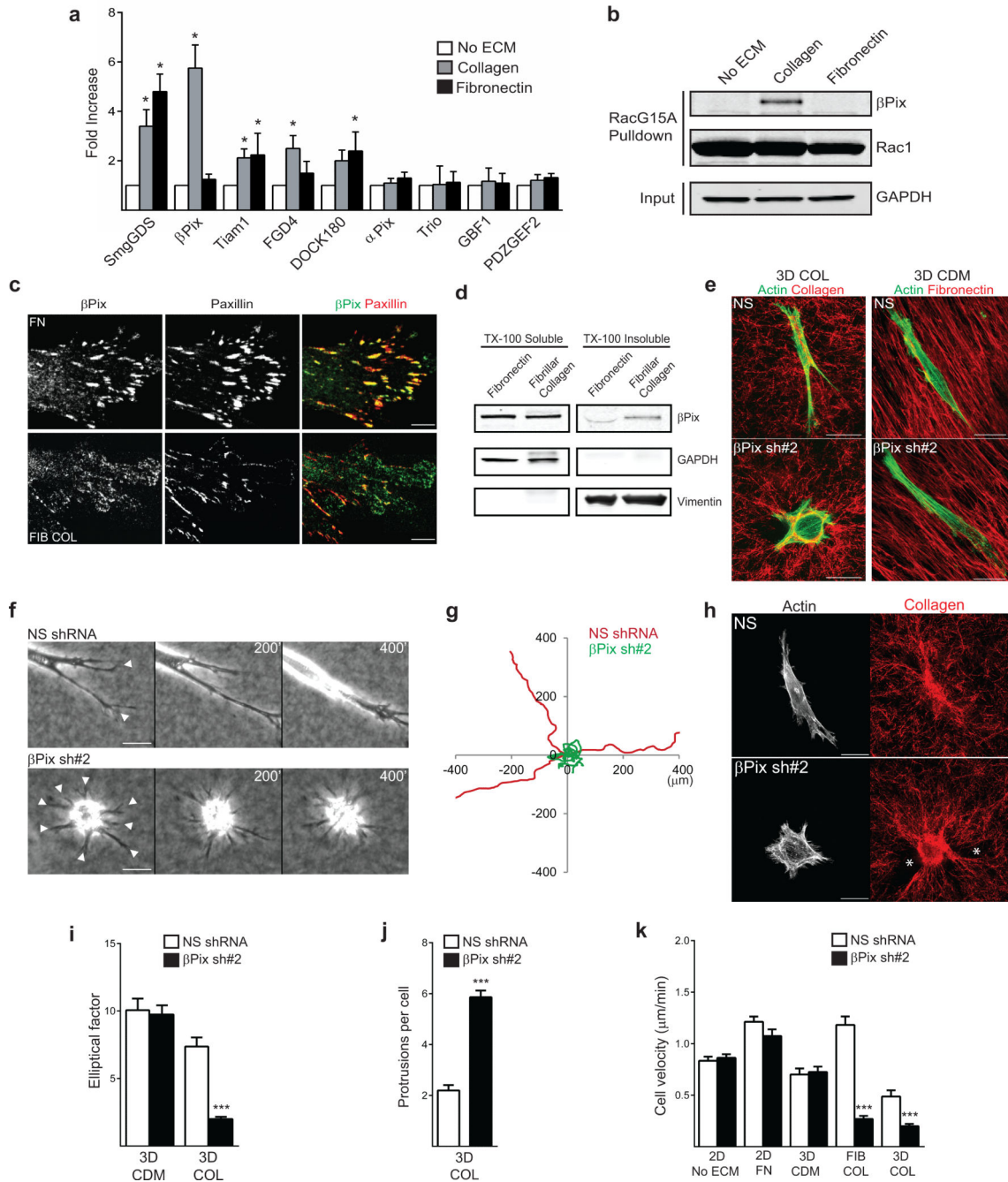
40. Hodgson L, Shen F, Hahn K. Biosensors for characterizing the dynamics of rho family GTPases in living cells. *Current protocols in cell biology* / editorial board, Juan S. Bonifacino ... [et al.]. 2010 Chapter 14, Unit 14 11 11-26.

Author Manuscript

Author Manuscript

Author Manuscript

Author Manuscript

**Figure 1.**

Loss of β Pix leads to collagen-specific morphological and migratory defects. **(a)** Quantification of western blot band intensities of select GEFs isolated from the RacG15A ECM-GEF screen. Values are fold intensity increase above No ECM condition; (n=3 independent western blots, mean \pm s.e.m, one-way ANOVA with Bonferroni multiple comparisons correction). **(b)** Western blot validation of β Pix binding to RacG15A during migration on collagen. **(c)** Composite images of the leading edge of HFFs show loss of β Pix localization to focal adhesions during migration on fibrillar collagen (FIB COL) but not

fibronectin (FN). HFFs were immunostained for endogenous paxillin (red) and β Pix (green); yellow indicates co-localization. See Supplementary Fig. 1d for the whole-cell images. Scale bars, 15 μ m. **(d)** Triton X-100 fractionation of HFFs migrating on fibronectin or fibrillar collagen reveals a shift of β Pix from soluble (GAPDH) to the insoluble (vimentin) fraction during migration on collagen, observed in three independent experiments. **(e)** Morphological analysis of β Pix knockdown in 3D fibrillar collagen (red, reflection microscopy) versus 3D cell-derived matrix (red, fibronectin) reveals defects in cell elongation after loss of β Pix specific to 3D collagen. Scale bars, 25 μ m. **(f)** Representative phase timelapse of nonspecific (NS) and β Pix shRNA fibroblasts migrating in 3D collagen. White arrowheads indicate cellular protrusions; scale bars, 25 μ m. **(g)** Migratory tracks of three NS (red) and β Pix (green) shRNA fibroblasts in 3D collagen reveal loss of persistent, directional motility after β Pix knockdown. **(h)** Analysis of collagen fibers (red, reflection microscopy) adjacent to NS and β Pix shRNA cells reveal robust collagen contraction and remodeling with β Pix knockdown (physical holes, asterisks). Scale bars, 25 μ m. **(i)** Quantification of cell elliptical factor (maximal length/width) in 3D collagen versus 3D cell-derived matrix after loss of β Pix. $n = 44, 46, 30,$ and 35 cells for NS CDM, β Pix sh#2 CDM, NS COL, and β Pix sh#2 COL were assessed across three independent experiments (mean \pm s.e.m., t -tests). **(j)** Quantification of cell protrusions (e, white arrowheads) after fixation and phalloidin staining of β Pix knockdown cells in 3D collagen. $n = 36$ cells for both NS and β Pix shRNA were assessed across three independent experiments (mean \pm s.e.m., t -tests). **(k)** Quantification of cell velocities after β Pix knockdown in different ECM conditions. $n = 20$ -25 cells for NS and β Pix shRNA in each matrix condition were assessed across three independent experiments (mean \pm s.e.m., t -tests). Statistical source data can be found in Supplementary Table 2. *** $P < 0.001$, * $P < 0.05$.

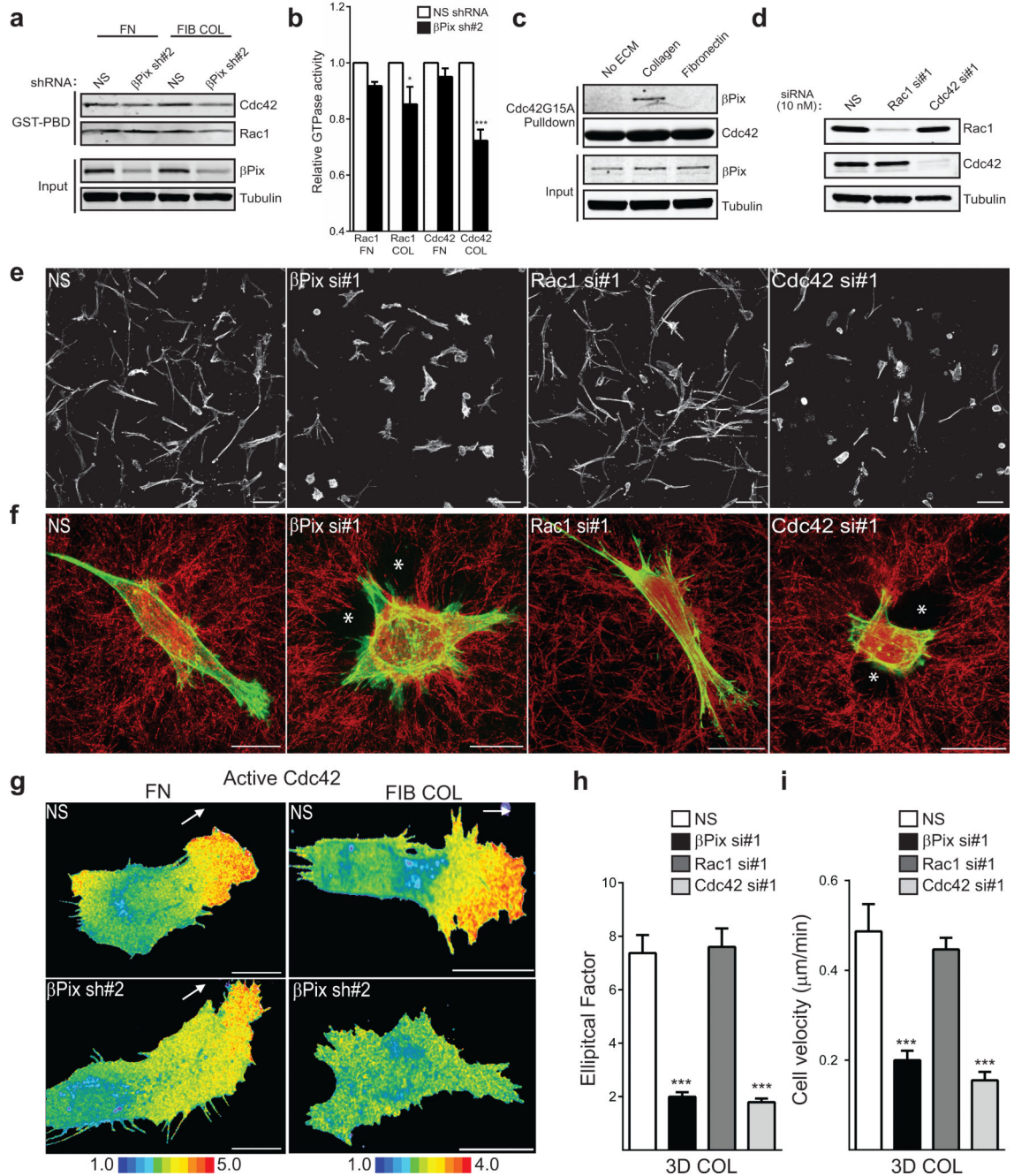


Figure 2.

βPix controls the activity and localization of Cdc42 during 3D collagen migration. **(a)** Active Rac1 and Cdc42 were isolated using GST-PBD from NS and βPix shRNA-expressing HFFs migrating on fibronectin (FN) or fibrillar collagen (FIB COL). **(b)** Quantification of western blot band intensity revealed collagen-specific losses in both Rac1 (~20%) and Cdc42 (~30%) activity after depletion of βPix (n = 3 independent western blots, mean ± s.e.m, *t*-tests). **(c)** βPix also binds specifically to recombinant Cdc42G15A in lysates from cells migrating on collagen, but not fibronectin. Result represents three independent

experiments. **(d)** Single, independent siRNA treatments (10 nM) targeting Rac1 or Cdc42 were sufficient to deplete endogenous protein levels. **(e)** siRNA-treated HFFs were embedded in 3D collagen gels and incubated overnight in complete media. Cells were then fixed and stained with rhodamine-phalloidin. Maximum projections of 150 μm sections of the actin-labeled gels revealed that knockdown of Cdc42 mimicked βPix knockdown morphology, with no defects observed with Rac1 knockdown. Scale bars, 50 μm . **(f)** Higher-power images of actin-labeled (green), siRNA-treated fibroblasts in relation to the surrounding collagen fibers (red, reflection microscopy). Knockdown of Cdc42 mimics the morphology, protrusive, and highly contractile phenotype of βPix knockdown. Holes torn in the collagen matrix are indicated by white asterisks; scale bars, 25 μm . **(g)** Maximum projections of confocal stacks of live-fibroblast migration expressing a Cdc42 biosensor on fibronectin or fibrillar collagen. Active Cdc42 is polarized toward the leading edges during migration on fibronectin in fibroblasts expressing NS or βPix shRNA. After knockdown of βPix on collagen, polarization of Cdc42 activity is lost, and overall activity is decreased. Pseudocolor intensity scales were maintained for each matrix condition; scale bars, 25 μm . White arrows designate direction of leading edge protrusions. **(h)** Quantification of cell elliptical factor (maximal length/width) in 3D collagen after Rac1 or Cdc42 siRNA treatments. $n = 35, 30, 35,$ and 31 cells for NS, βPix , Rac1, Cdc42 siRNA were assessed across three independent experiments. **(i)** Quantification of cell velocity in 3D collagen for Rac1 or Cdc42 siRNA treatments. $n = 25, 24, 22,$ and 24 cells for NS, βPix , Rac1, Cdc42 siRNA were assessed across three independent experiments. For **(h)** and **(i)**, data given as mean \pm s.e.m., one-way ANOVA with Bonferroni multiple comparisons correction. Statistical source data can be found in Supplementary Table 2, *** $P < 0.001$ * $P < 0.05$.

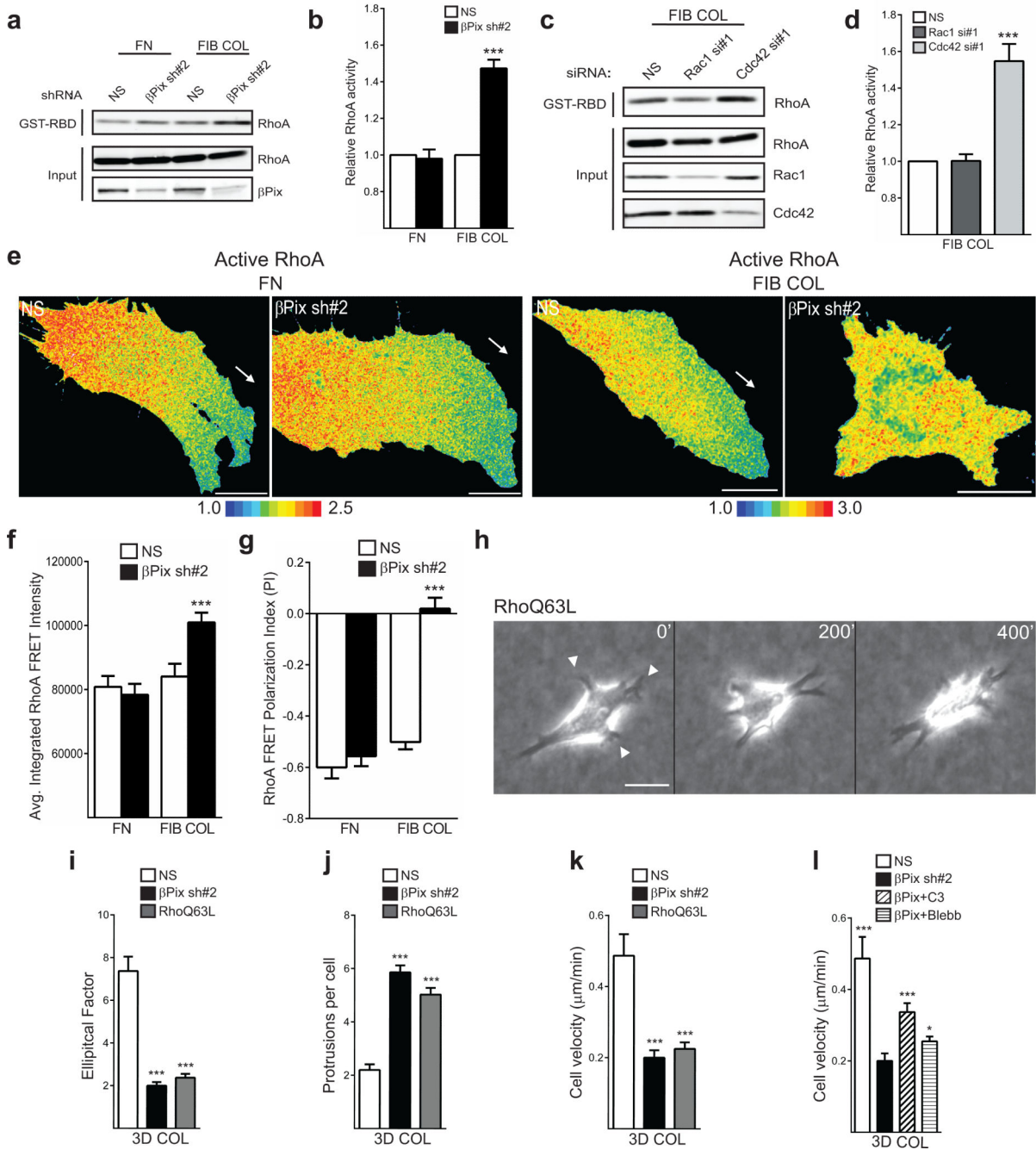
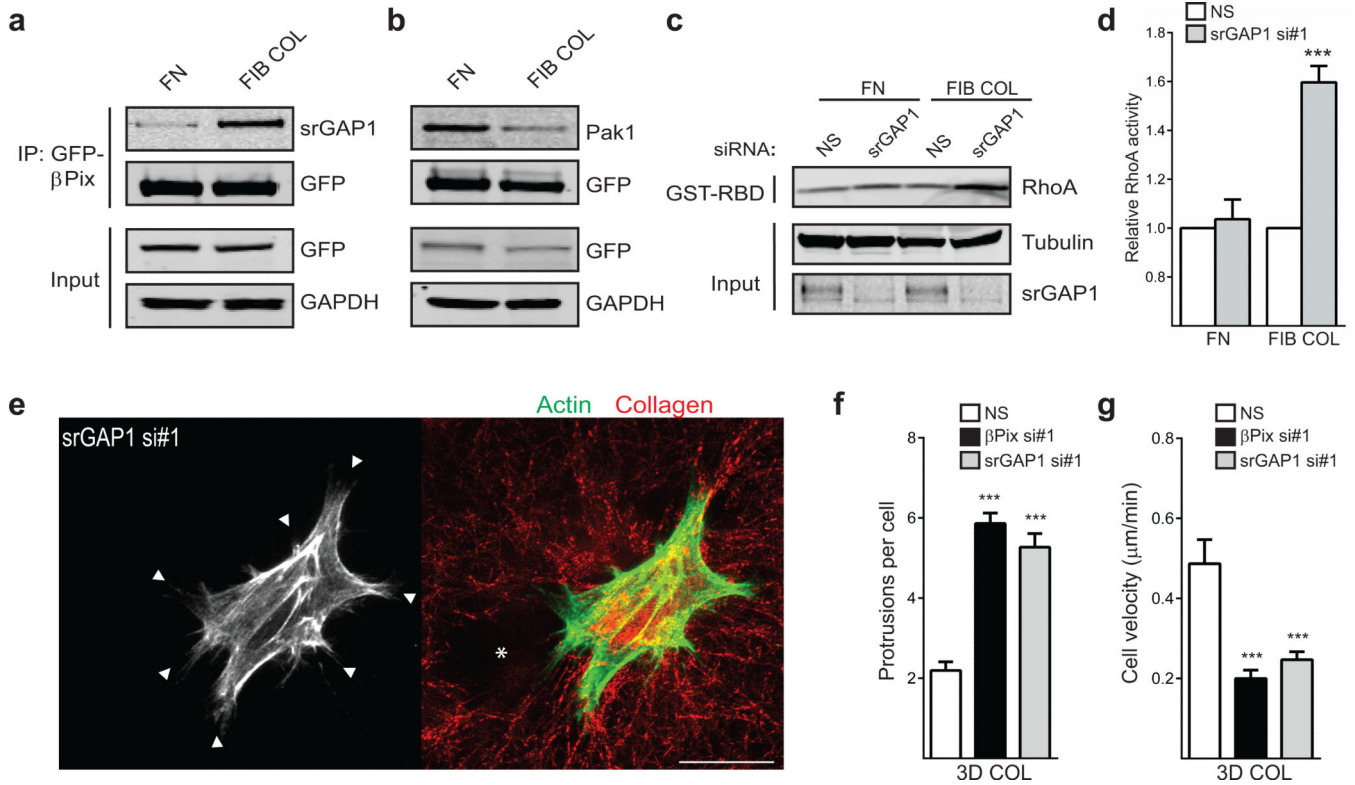


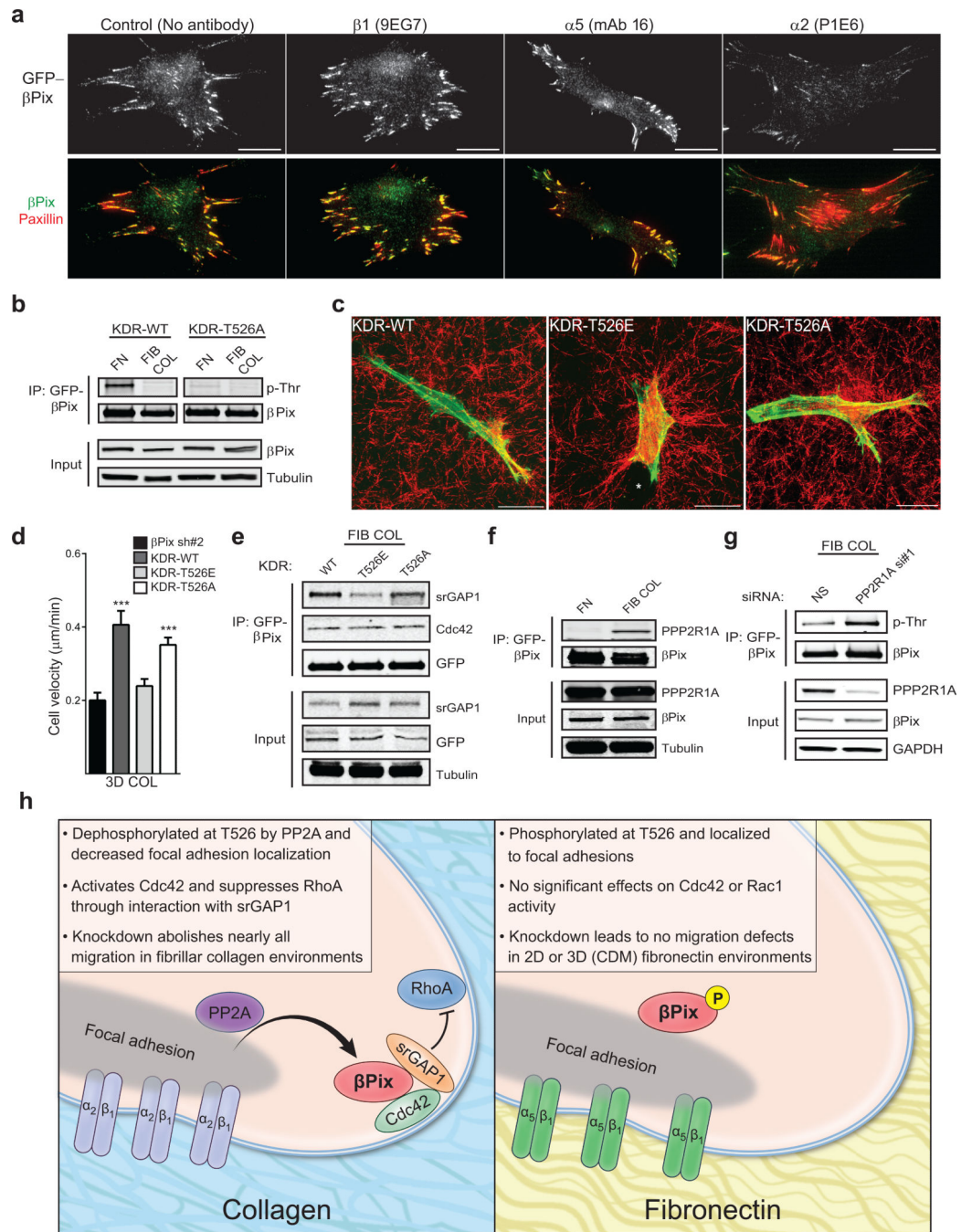
Figure 3.

βPix acts through Cdc42 to suppress and localize RhoA activity during migration in 3D collagen. **(a, b)** RhoA activity determined using GST-RBD binding from NS and βPix shRNA-expressing HFFs migrating in fibronectin or fibrillar collagen environments; collagen-specific increases (40-60%) in RhoA activity with loss of βPix (mean ± s.e.m, n = 3 independent western blots, *t*-tests). **(c, d)** Similarly, knockdown of Cdc42, but not Rac1, during migration on fibrillar collagen leads to increased intracellular RhoA activity (mean ± s.e.m, n = 3 independent western blots, one-way ANOVA with Bonferroni correction). **(e)**

Maximum projections of confocal stacks of live fibroblast migration expressing a RhoA biosensor on fibronectin (FN) or fibrillar collagen (FIB COL). Knockdown of β Pix on collagen results in overall elevation of RhoA activity accompanied by a loss of front-back segregation of RhoA activity. Pseudocolor intensity scales were identical for each matrix condition; scale bars, 25 μ m. White arrows designate direction of leading edge protrusions. **(f)** Average integrated whole cell RhoA FRET intensity on FN versus FIB COL. $n = 10$ cells for NS FN, β Pix sh#2 FN, NS FIB COL, and β Pix sh#2 FIB COL were assessed across three independent experiments (mean \pm s.e.m., t -test). **(g)** Quantification RhoA FRET polarization index on FN versus FIB COL. $n = 10$ cells for NS FN, β Pix sh#2 FN, NS FIB COL, and β Pix sh#2 FIB COL were assessed across three independent experiments (mean \pm s.e.m., t -test). **(h)** Phase contrast timelapse images (Supplementary Movie 4) of an HFF expressing low levels of GFP-RhoAQ63L in 3D collagen reveal rounded morphology, spatially and temporally deregulated protrusions (white arrowheads) and loss of persistent migration. Scale bars, 25 μ m. **(i)** Quantification of cell elliptical factor (maximal length/width) in cells low-expressing GFP-RhoAQ63L in 3D collagen. $n = 30, 35,$ and 29 cells for NS, β Pix sh#2, and RhoQ63L were assessed across three independent experiments. **(j)** Quantification of cell protrusions in cells with low-level GFP-RhoAQ63L expression in 3D collagen. $n = 36, 36,$ and 29 cells for NS, β Pix sh#2, and RhoQ63L were assessed across three independent experiments. **(k)** Quantification of cell velocity in cells with low GFP-RhoAQ63L expression in 3D collagen. $n = 25, 24,$ and 21 cells for NS, β Pix sh#2, and RhoQ63L were assessed across three independent experiments. **(l)** β Pix shRNA fibroblasts were cultured overnight in 3D collagen gels in the presence of cell-permeable C3 transferase (2 μ g/mL) or blebbistatin (25 μ M). $n = 25, 24, 20,$ and 20 cells for NS, β Pix sh#2, β Pix+C3, and β Pix +Blebb were assessed across three independent experiments. For **(i-l)**, data given as mean \pm s.e.m., one-way ANOVA with Bonferroni multiple comparisons correction. Statistical source data can be found in Supplementary Table 2, *** $P < 0.001,$ * $P < 0.05.$

**Figure 4.**

A collagen-specific GEF/GAP interaction between β Pix and srGAP1 regulates suppression of RhoA activity. **(a)** Immunoprecipitation of GFP- β Pix from β Pix knockdown/rescue HFFs migrating on fibronectin (FN) versus fibrillar collagen (FIB COL) identifies a collagen-specific GEF/GAP interaction between β Pix and srGAP1. **(b)** Concurrent decreased association of β Pix with known effector Pak1 when migrating on fibrillar collagen. Blots are representative of three independent experiments. **(c)** RhoA activity determined by GST-RBD binding from NS and srGAP1 siRNA-treated HFFs migrating on fibronectin or fibrillar collagen environments. **(d)** Quantification of bands again revealed a 40-60% collagen-specific increase in RhoA activity after loss of srGAP1 (mean \pm s.e.m., $n = 3$ independent western blots, t -tests). **(e)** srGAP1 knockdown HFFs were cultured overnight in 3D collagen gels. Fixation and labeling with Alexa488-phalloidin revealed a rounded, protrusive (white arrowheads) morphology akin to β Pix knockdown. Similarly, srGAP1 knockdown fibroblasts severely alter collagen fiber arrangement (red, reflection microscopy) adjacent to the cell. Hole in matrix marked by white asterisk; scale bar, 25 μ m. **(f)** Quantification of cell protrusions in cells treated with srGAP1 siRNA in 3D collagen. $n = 36, 36,$ and 24 cells for NS, β Pix si#1, and srGAP1 si#1 were assessed across three independent experiments (mean \pm s.e.m., one-way ANOVA with Bonferroni multiple comparisons correction). **(g)** Quantification of cell velocity in cells treated with srGAP1 siRNA in 3D collagen. $n = 25, 24,$ and 21 cells for NS, β Pix si#1, and srGAP1 si#1 were assessed across three independent experiments (mean \pm s.e.m., one-way ANOVA with Bonferroni multiple comparisons correction). Statistical source data can be found in Supplementary Table 2, *** $P < 0.001$.

**Figure 5.**

Fibrillar collagen activates β Pix through $\alpha_2\beta_1$ integrin, leading to a critical dephosphorylation at T526 through PP2A. (a) Loss of focal adhesion localization is a read-out of differential β Pix function on fibrillar collagen (Fig. 1c). Dishes were coated with monoclonal integrin antibodies targeting β_1 (9EG7), α_5 (mAb 16), or α_2 (P1E6) to mimic integrin ligation. GFP- β Pix knockdown/rescue cells were plated on the dishes and assayed for focal adhesion localization (red; yellow in overlay). Ligation of α_2 results in a dramatic loss in GFP- β Pix (grayscale) localization at paxillin (red)-containing adhesions with no

changes in overall focal adhesion profile. Scale bars, 25 μm . **(b)** Western blot of KDR-WT GFP- βPix immunoprecipitated from knockdown/rescue cells migrating on fibronectin or fibrillar collagen for phospho-threonine showed a decrease in phosphorylation levels during migration on collagen. Immunoprecipitation of KDR-T526A βPix showed no change in phospho-threonine between FN and FIB COL, highlighting the functional importance of this residue. **(c)** We generated phospho-mimetic (T526E) and phospho-null (T526A) mutant βPix knockdown/rescue cells and assayed their morphology in 3D collagen. T526E βPix was insufficient to rescue the morphological and hypercontractile phenotype of βPix knockdown (collagen fibers, red, reflection microscopy). T526A mutants efficiently rescued the βPix morphological and contractile defects. Scale bars, 25 μm . **(d)** Quantification of cell velocity in βPix knockdown/rescue phosphovariants in 3D collagen. $n = 25, 24, 22,$ and 22 cells for βPix sh#2, WT, T526E, and T526A were assessed across three independent experiments (mean \pm s.e.m., one-way ANOVA with Bonferroni multiple comparisons correction). **(e)** GFP- βPix was immunoprecipitated from HFFs expressing knockdown/rescue phosphovariants at Thr526 migrating on fibrillar collagen. We find that phosphorylationmimetic (T526E) inhibits binding to srGAP1, but not Cdc42. **(f)** Immunoprecipitation of GFP- βPix from βPix knockdown/rescue cells migrating on fibronectin versus fibrillar collagen identified a collagen-specific interaction between βPix and PP2A regulatory subunit A α isoform (PPP2R1A). **(g)** GFP- βPix knockdown/rescue fibroblasts migrating on fibrillar collagen were treated with NS or PPP2R1A siRNA #1. We observed that knockdown or inhibition (Supplementary Fig. 5g) of PPP2R1A increased phosphothreonine levels on βPix during migration on collagen. **(h)** Summary model of the collagen-specific role of βPix during migration in fibrillar collagen environments. All western blots are representative of at least three independent experiments. Statistical source data can be found in Supplementary Table 2, *** $P < 0.001$.